ACS APPLIED MATERIALS & INTERFACES

Research Article

www.acsami.org

Stabilizing Cu_2S for Photovoltaics One Atomic Layer at a Time

Shannon C. Riha,[†] Shengye Jin,[‡] Sergey V. Baryshev,[†,§,∥] Elijah Thimsen,[†,#,⊥] Gary P. Wiederrecht,[‡] and Alex B. F. Martinson*[,†]

[†]Materials Science Division and [‡]Nanoscience and Technology Division, Argonne National Laboratory, 9700 South Cass Avenue, Argonne, Illinois 60439, United States

Supporting Information

ABSTRACT: Stabilizing Cu_2S in its ideal stoichiometric form, chalcocite, is a long-standing challenge that must be met prior to its practical use in thin-film photovoltaic (PV) devices. Significant copper deficiency, which results in degenerate p-type doping, might be avoided by limiting Cu diffusion into a readily formed surface oxide and other adjacent layers. Here, we examine the extent to which PV-relevant metal-oxide over- and underlayers may stabilize Cu_2S thin films with desirable semiconducting properties. After only 15 nm of TiO_2 coating, Hall measurements and UV−vis−NIR spectroscopy reveal a significant suppression of free charge-carrier addition that depends strongly on the choice of deposition chemistry. Remarkably, the insertion of a single atomic layer of Al_2O_3 between Cu_2S and TiO_2 further stabilizes the active layer for at least 2 weeks, even under ambient conditions. The mechanism of this remarkable enhancement is explored by in situ microbalance and conductivity measurements. Finally, photoluminescence quenching measurements point to the potential utility of these nanolaminate stacks in solar-energy harvesting applications.

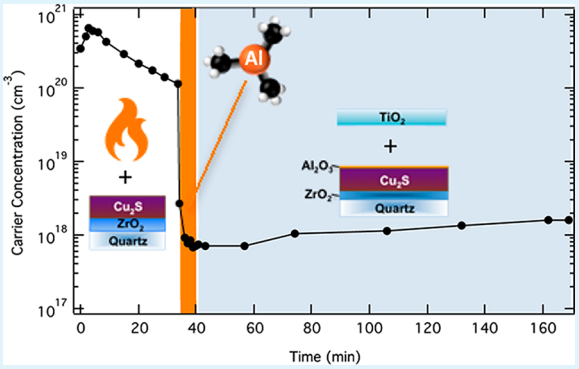

KEYWORDS: *copper sulfide, Cu_2S, atomic-layer deposition, thin-film solar cell, photovoltaic, barrier layers, surface passivation*

INTRODUCTION

Cu_2S was identified decades ago as a potential photovoltaic (PV) absorber because of its exceptional combination of nontoxicity, elemental abundance, and an absorption coefficient of $>10^4$ cm^{-1}. Owing to a 1.2 eV direct band gap, a theoretical single-gap PV efficiency greater than 30% is predicted, near the peak of the Shockley−Queisser detailed balance limit.[1−6] Historically, CdS/Cu_2S heterojunction PV devices reached pilot-line production efficiencies near 10% (at the time Si-based devices were around 11%).[7,8] Despite this rapid progress, several obstacles to long-term stability reduced interest in them in the late 1980s. Of major concern was the deterioration in the performance of the CdS/Cu_2S heterojunction device under ambient conditions, likely due to the instability of the Cu_2S active layer.[1,9−12] Early studies concluded that Cu diffusion, both into the CdS and to the surface oxides, transforms α-chalcocite (Cu_2S) into a heavily doped djurleite ($Cu_{1.96}S$), which decreases the device short-circuit current, open-circuit potential, and fill factor.[12]

At temperatures less than 90 °C, four distinct crystalline phases exist near Cu_2S: chalcocite (Cu_2S), djurleite ($Cu_{1.96}S$), digenite ($Cu_{1.8}S$), and anilite ($Cu_{1.75}S$).[13,14] The missing Cu^+ in substoichiometric $Cu_{2-x}S$ are compensated with an increase in free holes (intrinsic p-type dopants). Given approximately one positive free carrier per Cu vacancy, the formation of djurleite would lead to a carrier concentration $>10^{20}$ cm^{-3}, resulting in a degenerately doped semiconductor unsuitable for use in conventional PV applications.[15,16] Therefore, stabilizing the carrier concentration in stoichiometric Cu_2S is a prerequisite to the potential utilization of Cu_2S in practical PV.

Recently, we examined the intrinsic stability of model standalone Cu_2S thin films in nitrogen and air.[16] The electronic properties of the thin films were found to evolve rapidly under ambient atmospheres. The hole concentration, and therefore conductivity, rises by an order of magnitude immediately upon air exposure followed by a continued rise over weeks. Surface analysis revealed the formation of Cu_xO, in the form of a non-self-limiting oxide layer,[17,18] and X-ray diffraction indicated a simultaneous transformation from chalcocite to djurleite. Clearly, Cu_xO is formed from Cu^+ extracted from the bulk of the Cu_2S film, leaving behind Cu^+ vacancies that must be compensated with positive free charge carriers.[5,19] Calculations by Lukashev et al. suggest an intrinsic instability of stoichiometric Cu_2S (chalcocite), with the system favoring the formation of Cu vacancies (djurleite) even when in equilibrium with Cu metal.[5,20,21] Although neither an experimental verification nor quantification of any kinetics for this prediction have been reported, it is clear that vacancy formation is thermodynamically favorable in an oxidizing environment. Therefore, we hypothesize that inhibiting Cu

Received: August 4, 2013
Accepted: September 23, 2013
Published: October 10, 2013

reactions at the interface with air is paramount to maintaining moderate doping levels ($<10^{19}$ cm^{-3}) in thin films. Furthermore, it is well established that in addition to the formation of surface oxides Cu may also diffuse into some substrates or underlayers quite readily.[22] This represents a second potential diffusion pathway for Cu^+ out of Cu_2S. Cu diffusion has been a major concern in the microelectronics industry for some time, where Cu has been shown to diffuse readily into Si and SiO_2. As such, several approaches, including barrier layers, have been implemented to prevent the failure of integrated circuits.[18,23−26] Similarly, Cu has also been shown to diffuse in some transparent conducting oxides, highlighting the necessity for diffusion barriers in photovoltaic devices as well.[27,28]

Compared to metal sulfides, many metal oxides exhibit lower reactivity with atmospheric water and oxygen as well as orders of magnitude lower diffusion coefficients for metals like Cu. It is not surprising then that metal oxide over- and underlayers show promise for stabilizing metal sulfides. For example, Law and co-workers demonstrated that encapsulating lead chalcogenide nanoparticles in Al_2O_3 results in improved air stability and superior electronic properties.[29−31] Similarly, we previously showed that overcoating Cu_2S thin films with 30 nm of Al_2O_3 slows the degradation of the chalcocite phase by more than a factor of 100 compared to bare films.[16] However, although model Al_2O_3 overlayers serve to prove the concept, non-insulating (semiconducting) overlayers with similar effect would dramatically expand the range of functionality, including the potential for p−n junctions common to photovoltaics.[28]

Atomic-layer deposition (ALD) is an attractive route to both the preparation of pure and stoichiometric Cu_2S[16,32] as well as numerous metal-oxide layers. Unlike other deposition methods, the ALD mechanism involves two well-defined chemical half-reactions whereby two reactive vapor-phase chemical species are separated in time with inert-gas purging. As a result of the self-limiting half-reactions, the growth is digital, and the surface chemistry is well-defined. This affords unique opportunities to control the chemical bonding at the interfaces as well as the atomic-level thickness and composition control of films over large areas, even on substrates with complex geometry.[33−36] As such, we suggest that ALD is uniquely suited for several steps in the fabrication and understanding of Cu_2S thin-film PV devices, from nanostructuring the active layer to pinhole-free deposition of a heterojunction mate.

Here, we probe the effect of metal-oxide over- and underlayers of relevance to PV on the electronic stability of Cu_2S thin films. A ZrO_2 control and n-type TiO_2 overlayer are observed to consistently slow the rise in carrier concentration using thicknesses of order 20 nm. Strikingly, the addition of one ALD cycle of Al_2O_3 between these layers completely halts the rise in carrier concentration for at least 2 weeks. An in situ growth and conductivity study revealed a possible mechanism for this effect, and XPS data corroborate the suppression of Cu diffusion through this passivation layer. Finally, photoluminescence measurements demonstrate the potential for utilizing these nanolaminate stacks in PV devices.

METHODS

Thin-Film Deposition. A Cambridge Nanotech Savannah 200 ALD coupled to a N_2-filled glovebox and customized for compatibility with H_2S[37] was used for the deposition of all materials in the nanolaminate stack. The pulsing scheme for the depositions detailed below is as follows: t_1−t_2−t_3−t_4, where t_1 and t_3 are the pulse times and t_2 and t_4 are the purge times in seconds for the metal and oxidant precursor, respectively. Bis(*N*,*N*′-disec-butylacetamidinato)dicopper-(I) (CuAMD) and nickel amidinate (NiAMD) were purchased from Dow Chemical Company (Electronic Materials Division). Titanium tetraisopropoxide (TTIP), tetrakis(dimethylamido)titanium(IV) (TiTDMA), tetrakis(dimethylamido)zirconium(IV) (ZrTDMA), and trimethylaluminum (TMA) were purchased from Aldrich. H_2S (1%) in N_2 was used as the S source. (*Safety note: H_2S is a poisonous gas but it not flammable at a 1% concentration.*) All ALD precursors were used as received with no further purification. Cu_2S thin films were deposited using CuAMD, heated to 145 °C, and H_2S with a pulsing sequence of 2−20−0.1−20 at a reactor temperature of 130 °C. The precursor manifold was set to 150 °C to prevent precursor condensation prior to expansion into the ALD chamber. All over- and underlayers were deposited at a reactor temperature of 200 °C with the manifold at 150 °C. Al_2O_3 was deposited using TMA and DI water with 0.015 s pulses and 10 s purge steps for each precursor. TiO_2 deposited with TTIP (80 °C) and DI water was grown with the sequence 0.1−10−0.015−10. The sequence for growing TiO_2 using TiTDMA (75 °C) was identical to the TTIP recipe, with the exception that a 0.15 s pulse was used for TiTDMA. ZrTDMA (75 °C) and DI water were used for the growth of ZrO_2, with a pulsing sequence of 0.4−10−0.015−10. NiO was grown using 2.5−30−0.030−30 with NiAMD and DI water.[38] Fused quartz and silicon substrates were solvent-cleaned using a sequential 10 min sonication in acetone, 10 min sonication in isopropanol, and blow drying with N_2.

Characterization. Hall measurements were recorded at room temperature with an Ecopia HMS-3000 Hall measurement system. The probe current was selected such that the voltage signal was between 0.1 and 1 V. In some cases, the carrier concentration was derived from the measured conductivity values using a mobility of 5 cm^2 V^{-1} s^{-1}. This mobility was determined by room-temperature, inert-atmosphere Hall measurements on pristine ALD-Cu_2S thin films. In situ current−voltage (*I*−*V*) measurements were collected using a custom-built substrate holder that consisted of a Macor base with a cutout for the substrate (Figure S1). A metal foil was attached to the back to provide heat conduction to the substrate, and two leads were fastened to the Macor to prevent shorting to the metal foil. Teflon-insulated wires were attached to the leads and fed downstream through the exhaust line to a KF feedthrough that was further attached to a CHI 620D potentiostat. Film thicknesses were determined either from profilometry, ellipsometry, or by in situ quartz crystal microbalance (QCM) measurements. In situ QCM was performed using a custom-built ALD lid with two QCM ports installed 2 and 6 in. from the inlet port.[39] Reflectance-corrected UV−vis−NIR was collected on a Varian Cary 5000 with an integrating sphere accessory (DRA-2500). A custom X-ray photoelectron spectroscopy (XPS) instrument[40] with a Mg Kα (1253.6 eV) X-ray source and hemispherical electron-energy analyzer in the fixed absolute resolution mode was used for surface analysis of the nanolaminate stacks. Survey spectra were collected using a 44 kV pass energy, and detailed high-resolution spectra were collected using a 22 kV pass energy. The energy step for the survey and high-resolution spectra were 0.5 and 0.1 eV, respectively. CasaXPS (Casa Software, Ltd.) was used to analyze the data. All spectra were shifted using the Au $4f_{1/2}$ XPS emission line (with a binding energy of 84.0 eV). Scanning electron microscopy (SEM) images were collected on a Hitachi S4700-IL. The emission spectra of the nanolaminate stacks were measured on a home-built system. The samples were excited with a CW diode laser at 800 nm (50 mW), and the resulting photoluminescence spectra were collected by an optical lens, which was then focused on a monochromator (an InGaAs photodiode array from Princeton Instruments, 1 × 1024 pixels, 2 s integration).

RESULTS AND DISCUSSION

Metal-Oxide Over- and Underlayers. Alternating exposures of CuAMD and H_2S were used to deposit 100 nm thin films of Cu_2S. Although less relevant for PV applications, ZrO_2 over- and underlayer controls (at the Cu_2S/air or quartz/Cu_2S interface, respectively) were tested owing to the ease with

which they may be deposited by ALD as well as previous reports of its use as a diffusion barrier for Cu.[41] ZrO_2 under- or overlayers (or both) were deposited, and the stacks were subsequently exposed to ambient laboratory conditions. The largest improvement in the electronic properties of the Cu_2S thin film was achieved when using a 100 cycles (~12 nm) overlayer of ZrO_2, Figure 1. In contrast, 20 cycles (~3 nm) of

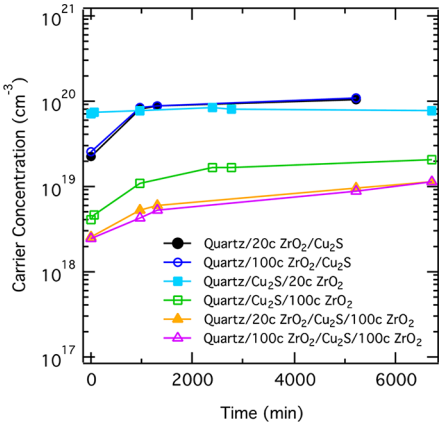

Figure 1. Carrier concentration derived from the conductivity determined by room-temperature Hall measurements for various combinations of ZrO_2 under- and overlayers.

ZrO_2 was insufficient to improve stability. No carrier stabilization can be resolved when adding only a ZrO_2 underlayer, as evidenced by the ~10^{20} cm^{-3} carrier concentration and >100 Ω^{-1} cm^{-1} conductivity. However, a significant enhancement is observed when a 3 or 12 nm thick ZrO_2 underlayer is utilized in addition to the 12 nm overlayer. As expected from prior literature,[18,23−26] the most dramatic slowing of p-type carrier addition is achieved by incorporating both an over- and underlayer. Although the Cu_2S/air interface shows a dominant effect, the most significant reduction in carrier rise is imparted by addressing both pathways for Cu^+ extraction.

Unlike ZrO_2, TiO_2 has potential to serve as both a diffusion barrier and n-type mate to Cu_2S in a heterojunction PV.[26] TiO_2 is abundant, stable, and environmentally benign, making it considerably more appealing than CdS, an n-type emitter commonly used in thin-film solar cells. Moreover, diffusion into metal oxides is generally orders of magnitude slower than into sulfides.[28] TiO_x, in particular, has been previously shown to act as a diffusion barrier for Cu interconnects.[18]

To compare effectively the results obtained with ZrO_2 over- and underlayers to that obtained with TiO_2, a "reset" process was developed that enables the use of Cu_2S films other than those freshly prepared. If the Cu_2S surface and carrier concentration could be recovered by post-treatment, then a large batch of Cu_2S substrates could be stored and later modified and compared with high precision. Previous reports indicate that thermal treatments of CdS/Cu_2S in air, under vacuum, or in a more reducing atmosphere (i.e., H_2 or CO) enhanced PV-device performance. The enhancement was attributed to optimizing the CdS/Cu_2S interface by essentially resetting the Cu_2S stoichiometry.[7,11,42−44] After aging in a N glovebox between 2 h and 1 month, the carrier concentrations of Cu_2S films ranged from the mid 10^{19} to low 10^{20} cm^{-3}, respectively. Aged samples were placed in the ALD chamber at 200 °C for 15, 30, or 60 min under 1 Torr of flowing ultrapure N_2.[7,42] Hall measurements were taken in the glovebox immediately after removal from the ALD reactor. In all cases, the carrier concentration was reduced to the low to mid 10^{18} cm^{-3} range, suggesting that this approach, even in the absence of a strongly reducing atmosphere, yields films similar to those freshly prepared. XPS analysis (Supporting Information, Figure S2) further suggests a recovery of the original surface chemistry, including the decomposition of surface oxides,[45,46] that are correlated with a return to the original electronic properties.

For Cu_2S films deposited on 12 nm ZrO_2-coated quartz, the process chemistry used for the deposition of TiO_2 overlayers impacted the stability of Cu_2S. Two well-known chemical precursors for TiO_2 ALD were investigated, TTIP and TiTDMA. A 15 nm TiO_2 film was deposited on either freshly prepared Cu_2S thin films immediately after Cu_2S deposition (without breaking vacuum) or on glovebox-stored films that were subject to a 30 min thermal reset as described above. The resulting properties and behavior of the nanolaminates based on fresh and reset Cu_2S films were indistinguishable. Figure 2a

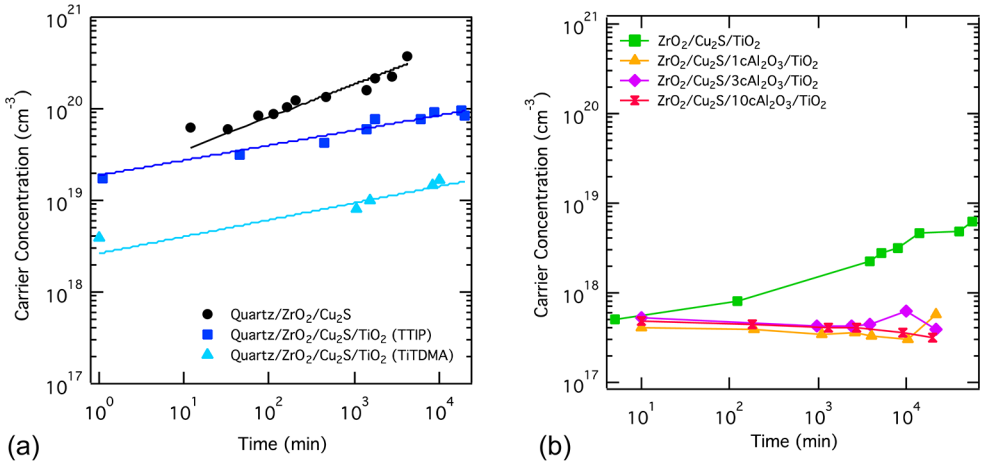

Figure 2. (a) Comparison of the carrier concentrations directly measured from 100 nm Cu_2S thin films passivated with ~15 nm TiO_2. The TiO_2 was grown with TTIP or TiTDMA. The rates of degradation can be found in Table S1. (b) TiO_2 grown using TiTDMA with 1, 3, or 10 cycles of Al_2O_3 included at the interface of Cu_2S/TiO_2. Because of the low conductivity of the samples in panel b, the carrier concentration was calculated from the conductivity determined from Hall measurements using a mobility of 5 cm^2 V^{-1} s^{-1}.

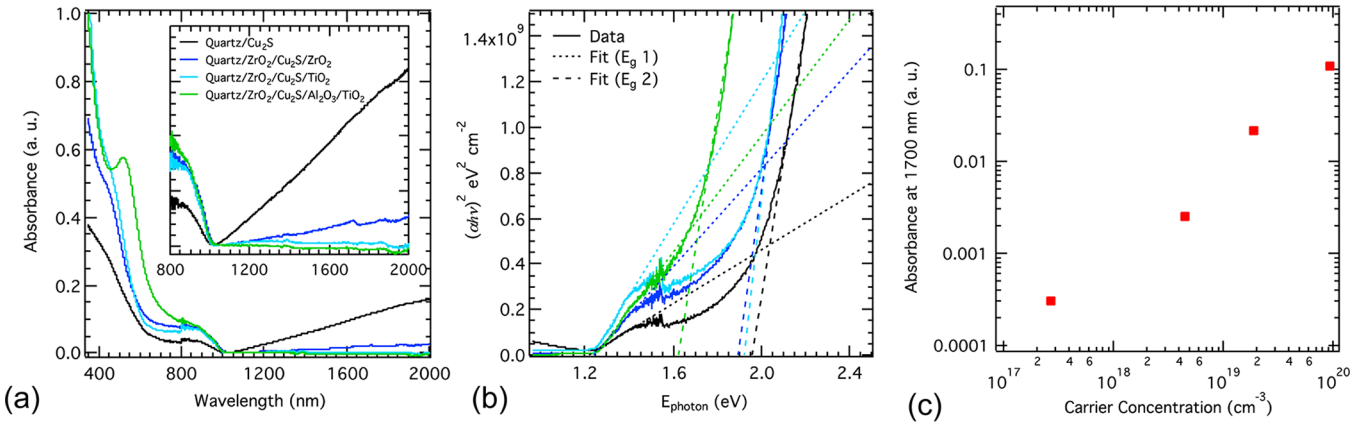

Figure 3. (a) UV–vis–NIR spectra and (b) Tauc plot for quartz/Cu_2S (black), quartz/ZrO_2/Cu_2S/ZrO_2 (blue), quartz/ZrO_2/Cu_2S/TiO_2 (aqua), quartz/ZrO_2/Cu_2S/Al_2O_3/TiO_2 (green). The inset in panel a shows the NIR absorption of each thin-film stack in more detail. In panel b, the dotted and dashed lines are fits to derive the direct band gap values. (c) Absorption at 1700 nm plotted as a function of the measured carrier concentration by room-temperature Hall measurements: quartz/ZrO_2/Cu_2S (10^{20} cm^{-3}), quartz/ZrO_2/Cu_2S/ZrO_2 (10^{19} cm^{-3}), quartz/ZrO_2/Cu_2S/TiO_2 (10^{18} cm^{-3}), and quartz/ZrO_2/Cu_2S/1cAl_2O_3/TiO_2 (10^{17} cm^{-3}).

shows the influence of TiO_2 overlayers, deposited using either TTIP or TiTDMA with H_2O, on the electronic stability of Cu_2S in air.

When TTIP was employed, the carrier concentration was found to be initially lower than an analogous quartz/ZrO_2/Cu_2S film without a TiO_2 overlayer, but the carrier concentration rapidly approached 10^{20} cm^{-3} (see Table S1). The initial carrier concentration and conductivity values were both reduced when the TiTDMA/H_2O process was used. The rate of free carrier addition was further suppressed (Table S1), and the carrier concentration of the Cu_2S films, passivated by TiO_2 grown with TiTDMA, remained lower than those passivated with TTIP-TiO_2. These values were also more than an order of magnitude lower than the unpassivated quartz/ZrO_2/Cu_2S films. We speculate that in the case of growing TiO_2 with TTIP the oxygen in the metal precursor may have a role to play, potentially through the release of ROH byproducts that may react with the Cu_2S layer early in the growth.

During the development of the reset process, it was discovered that a further reduction in the carrier concentration, to high 10^{16} or low 10^{17} cm^{-2}, prior to the addition of TiO_2 overlayers could be achieved after just one cycle of alumina (TMA + H_2O). Unfortunately, Cu_2S films solely treated in this way quickly increased in carrier concentration. However, the discovery inspired the addition of an ultrathin Al_2O_3 layer between the Cu_2S and top TiO_2. Prior to TiO_2 deposition via TiTDMA/H_2O, the nanolaminate stacks were subjected to a 30 min thermal reset at 200 °C under vacuum. Without breaking vacuum, 1, 3, or 10 ALD cycles of Al_2O_3 were deposited immediately followed by ∼15 nm of TiO_2 at 200 °C. Hall measurements, plotted in Figure 2b, revealed that with only one cycle of Al_2O_3 prior to TiO_2 deposition the addition of free carriers could be virtually halted for the duration of the measurements (a period of 2 weeks). That there is virtually no increase of free carriers in the samples with Al_2O_3/TiO_2 overlayers suggests stabilization on much longer time scales. Interestingly, one ALD cycle produces almost the same effect as three or even 10 ALD cycles of Al_2O_3. Although a subsequent in situ QCM study (vide infra) suggests that very little Al_2O_3 film growth occurs in the first five-to-six cycles, it is clear that even one cycle of Al_2O_3 had a dramatic effect on passivation performance. One hypothesis consistent with these observations is a change in the TiO_2 nucleation and grain growth behavior on Cu_2S with and without Al_2O_3 treatment, which might lead to significantly different passivation. It is notable, however, that when TTIP was used in conjunction with Al_2O_3 cycles the Cu_2S carrier concentration still rapidly reached 10^{19} cm^{-3} within 15 h.

The accuracy of the Hall measurement depends upon four relatively low-resistance contacts to the Cu_2S thin film, which is buried under a thin oxide overlayer in the above experiments. In cases where significant conductivity originates from the overlayer (this was found not to be the case for the thin and lightly doped TiO_2 films studied herein), the direct measurement would be further complicated. Therefore, to corroborate the results of the Hall measurements, NIR optical spectroscopy was also performed on the various nanolaminate stacks. It has been previously shown that upon oxidation of Cu_2S nanoparticles, NIR absorption results from free carrier absorption.[47−51] Therefore, a qualitative investigation of the NIR, alongside less dramatic differences in the visible wavelengths region reported for differing $Cu_{2-x}S$ phases, allows for a contactless probe of carrier concentration. Figure 3 plots the reflection-corrected UV–vis–NIR absorption of unpassivated quartz/Cu_2S, quartz/ZrO_2/Cu_2S/ZrO_2, quartz/ZrO_2/Cu_2S/TiO_2, and quartz/ZrO_2/Cu_2S/Al_2O_3/TiO_2 nanolaminate stacks. The Hall measurement-derived carrier concentrations were of the order 10^{20}, 10^{19}, 10^{18}, and 10^{17}, respectively. In all samples, a direct band gap of 1.2 eV was determined from the Tauc plot in Figure 3b. A second direct band gap was also inferred that is ∼0.65 eV higher in energy. Previous experimental observations, as well as recent calculations, suggest that this higher-energy transition originates from excitation to a second conduction band level located ∼0.6 above the first.[5,53] The blue shift in the band gap with increasing carrier concentration can be attributed to increasing Cu vacancies that reduce number of carriers in the valence band thereby open up the band gap, which is consistent with prior literature reports.[5,52] The inset in Figure 3a clearly depicts an absorption increase in the NIR that scales with the carrier concentration. A linear relationship between the absorbance at 1700 nm and the free carrier concentration derived from Hall measurements is shown as Figure 3c. This agreement between

optical spectroscopy and Hall measurements suggests that the metal oxide over- and underlayers significantly stabilize the electronic properties of the Cu_2S layers by reducing or halting the formation of free carriers that result from surface oxidation and Cu diffusion.

In Situ Analysis of ALD Overlayers. To understand the origins of this remarkable stabilization effect, in situ QCM (Figures 4 and S3) and current−voltage (I−V) measurements

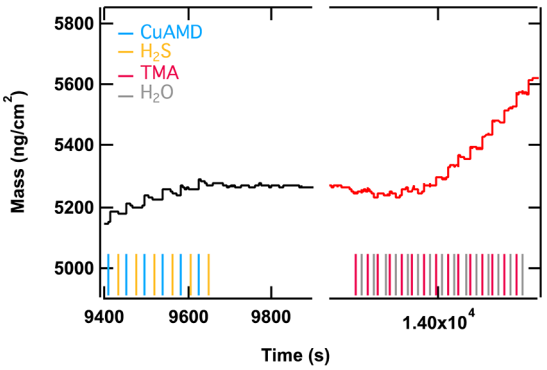

Figure 4. In situ QCM measurement monitoring the deposition of Al_2O_3 on Cu_2S after venting the ALD to the glovebox atmosphere for 2 h, raising the temperature of the ALD to 200 °C, and equilibrating for 1 h at temperature under vacuum. The black trace is the last six cycles of Cu_2S, with the blue and yellow tick marks corresponding to the CuAMD and H_2S precursors, respectively. The red QCM trace plots the Al_2O_3 deposition, where the red and gray tick marks are the TMA and H_2O pulses, respectively.

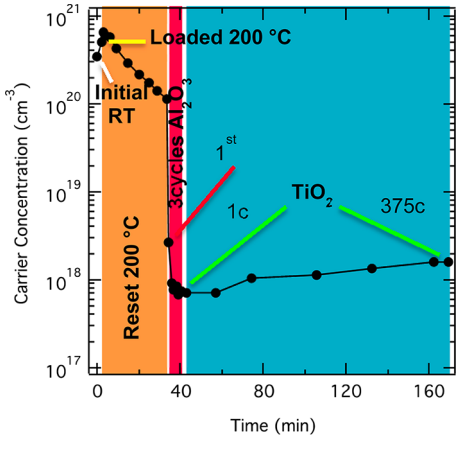

Figure 5. Carrier concentrations, calculated from in situ I−V measurements, vs time during the reset process and subsequent deposition of the quartz/ZrO_2/Cu_2S/3cAl_2O_3/TiO_2 stack. The orange, magenta, and aqua regions highlight the reset process, three cycles of Al_2O_3, and TiO_2 deposition, respectively. Carrier concentrations are an estimate on the basis of the resistance at 0.2 V, a presumed carrier mobility of 5 $cm^2\ V^{-1}\ s^{-1}$, and assuming a Cu_2S thickness of 100 nm.

(Figures 5 and S4) were performed during film growth and processing. Cu_2S was deposited onto the quartz crystals, and the chamber was then vented to the glovebox atmosphere. The QCM lid was cooled and exposed to the glovebox atmosphere for 2 h before pumping to vacuum and ramping the ALD temperature to 200 °C, processing very similar to that for the samples investigated in the previous section. After thermal equilibration for ∼1 h, several Al_2O_3 ALD cycles were performed at 200 °C. The resulting mass changes are presented in Figure 4. A small mass loss was observed simultaneous with the first TMA pulse, corresponding to what would be a 0.3 Å (assuming a density of 5.6 g/cm^2) reduction in Cu_2S or Cu_2O. Clear Al_2O_3 growth has a pronounced nucleation delay, with no obvious mass addition for at least five cycles. These results do not, however, exclude the possibility that Al_2O_3 growth may be displacing surface oxides or residual precursor ligands. Although the chemical bonding between relevant atoms (Cu, S, Al, and O) is inaccessible at this stage, the surface chemistry of this interface is the subject of further investigations in our lab.

To capture the distinct change in conductivity observed ex situ above, in situ I−V measurements were also performed under processing conditions commensurate with those used to prepare the most stable Cu_2S nanolaminate stacks. In situ I−V measurements were executed during the 30 min thermal reset process and subsequent overlayer deposition (using three cycles of Al_2O_3 and 15 nm TiO_2 at 200 °C). Figure 5 shows the estimated carrier concentration versus time, calculated from the resistance at 0.2 V (Figure S4) and assuming a Cu_2S thickness of 100 nm and carrier mobility of 5 $cm^2\ V^{-1}\ s^{-1}$, for quartz/ZrO_2/Cu_2S/3cAl_2O_3/TiO_2. During the thermal treatment under vacuum, the carrier concentration in both samples decreased as expected. In Figure 5, the carrier concentration decreased throughout the 30 min thermal reset, reducing the value by 5-fold during the 200 °C soak. Instantaneous with the first TMA dose, the carrier concentration further decreased by over an order of magnitude. A saturating carrier concentration was achieved after two cycles of Al_2O_3, with a minimum value ∼2 orders of magnitude lower than a Cu_2S sample with thermal reset alone. Deposition of TiO_2 induced only minimal changes to the carrier concentration. Upon cooling the sample to room temperature, the carrier concentration estimated from the resistance was in accordance with values determined by Hall measurements (10^{17} cm^{-3}). The combination of in situ I−V and ex situ Hall measurements begin to map the effects of heat treatment under vacuum and subsequent ALD precursors with high resolution. Furthermore, we begin to visualize any changes to the Cu_2S thin film and potentially the formation of a p−n junction. A more detailed in situ study with chemical insights, perhaps via quadrupole mass spectrometry to determine gas-phase products, is warranted to derive further details of the mechanism behind Cu_2S surface modification and junction formation.[54,55] Such studies are, however, beyond the scope of this report, which is to describe the effects of various treatments on materials properties.

Surface Analysis. The exposure of Cu_2S to at least one TMA/H_2O cycle prior to TiO_2 overcoating has two distinct and important effects. First, TMA exposure clearly reduces the initial number of free charge carriers in the chalcocite film by more than an order of magnitude. Second, the modification dramatically improves the effectiveness of a subsequent TiO_2 overlayer. We hypothesize that the TMA/H_2O treatment provides a more robust and uniform interface between Cu_2S and TiO_2, which may reduce the formation of a non-self-limiting CuO_x layer at the interface[56] and/or enable a more complete and pinhole-free TiO_2 overlayer. As one of the most sensitive probes to surface composition, XPS was undertaken to examine whether Cu diffused to the surface of the glass/ZrO_2/Cu_2S/TiO_2 nanolaminate stacks prepared with and without an intermediate single cycle of Al_2O_3. The samples were stored

under ambient conditions for 8 days prior to XPS analysis. Figure 6a shows the survey scan for each nanolaminate stack,

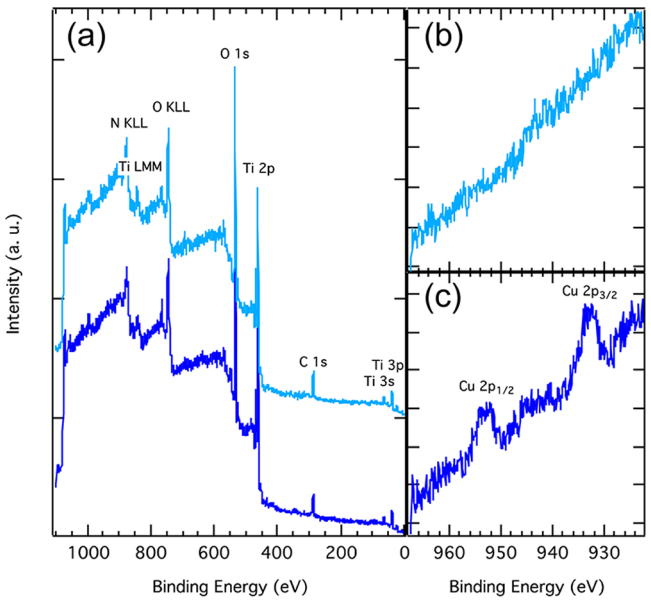

Figure 6. XPS data for quartz/ZrO_2/Cu_2S/TiO_2 (blue) and quartz/ZrO_2/Cu_2S/Al_2O_3/TiO_2 (aqua). (a) Survey scan of both samples and high-resolution scan of (b) quartz/ZrO_2/Cu_2S/Al_2O_3/TiO_2 and (c) quartz/ZrO_2/Cu_2S/TiO_2.

whereas panels b and c are high-resolution scans of the Cu 2p region with and without the TMA/H_2O treatment, respectively. Despite the TiO_2 overlayer, Cu is present on the surface of the nanolaminate stack when an Al_2O_3 interfacial layer is omitted. This is consistent with the depletion of Cu from Cu_2S as inferred from Hall measurements (Figure 2b). Although Cu diffusion through a uniform and pinhole-free TiO_2 overlayer cannot be excluded, the observation of Cu on the nanolaminate surface suggests that the TiO_2 growth is nonuniform. Island growth, in contrast to continuous thin-film deposition, is not uncommon for ALD oxides grown on surfaces with low nucleation density, which may result from incompatible surface chemistry (in this case, a lack of hydroxyl termination). In contrast, no Cu was observed at the surface of the nanolaminate stack when one cycle of Al_2O_3 was introduced prior to overcoating with TiO_2. This is consistent with our hypothesis that the TMA/H_2O treatment improves the homogeneity of TiO_2 nucleation and subsequent continuous thin-film growth. A similar morphological effect, in which a few cycles of TMA/H_2O has improved the nucleation of subsequent oxides, has been previously observed in related systems.[57]

Photoluminescence. The next step toward the identification of a nanolaminate stack suitable for use in solar-energy conversion is an understanding of the photoinduced charge-separated state. Steady-state and time-resolved photoluminescence (PL) spectroscopies are common and useful routes to information about minority carrier lifetimes, interfacial charge transfer, and the surface recombination velocity.[58−60] Such studies are particularly informative when correlated with the electronic properties and diverse under- and overlayers investigated herein. In addition to those stacks described above, Cu_2S interfaces with NiO were also prepared. As an intrinsically p-type oxide with band alignment suitable to accept holes from Cu_2S, NiO was used in place of ZrO_2 at the quartz/Cu_2S interface in some samples. On the basis of Hall measurements and UV−vis−NIR data, the quartz/NiO/2cAl_2O_3/Cu_2S/1cAl_2O_3/TiO_2 nanolaminate stack demonstrated similar stability under ambient conditions to the quartz/ZrO_2/Cu_2S/1cAl_2O_3/TiO_2 nanolaminate. As a preliminary study of the photoinduced charge-separated state, the steady-state PL spectra and relative intensity for various nanolaminate stacks with 150 nm thick Cu_2S films were measured (Figures 7

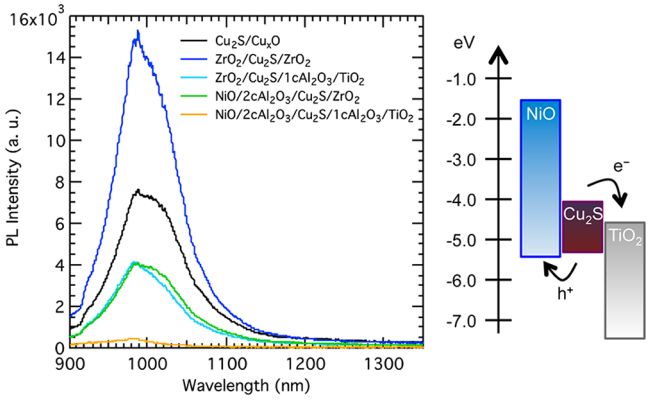

Figure 7. Room-temperature PL spectra of various nanolaminate stacks with 150 nm Cu_2S. The right panel depicts an idealized energy-level diagram prior to equilibration for the quartz/NiO/2cAl_2O_3/Cu_2S/1cAl_2O_3/TiO_2 stack.

and S5). The most intense PL was recorded for a Cu_2S film sandwiched by ZrO_2. With band edges predicted to be inaccessible to either electron or hole injection from Cu_2S, this result is not unexpected. The PL spectra peaks around 1.27 eV, consistent with previous reports of stoichiometric chalcocite.[48,61] The emission is centered near the absorption band edge and lacks any lower-energy peaks that might be indicative of intragap states. The native oxides that grow on Cu_2S under ambient conditions also preserve significant PL despite the strong electronic effects of Cu vacancy formation in the underlying Cu_2S. This suggests a moderate surface-recombination velocity at this interface, which might be anticipated based on reports of the most efficient Cu_2S PV to date that are likely terminated with a similar interface.[44,62] With a 1cAl_2O_3/TiO_2 overlayer, the PL intensity significantly decreases relative to the ZrO_2-sandwiched film. This behavior is consistent with, but not proof of, charge-transfer quenching that may be predicted given the expected energy-level alignment (Figure 7, right). The PL intensity and rationalization is similar for the case of a NiO underlayer, except that hole transfer is anticipated. Less than 4% of the original PL intensity remains for the quartz/NiO/2cAl_2O_3/Cu_2S/1cAl_2O_3/TiO_2 nanolaminate stacks. Although there are other possible explanations for these trends, they are consistent with a charge-transfer mechanism in which excited electrons in Cu_2S are injected into the TiO_2, whereas the holes are injected into the NiO. Together with the electrical studies above, these results bolster the prospects for an air-stable nanolaminate stack with the potential for application in solar-energy conversion.

CONCLUSIONS

Insulating and semiconducting metal-oxide thin films under and over Cu_2S thin films were investigated in an effort to minimize Cu diffusion and thereby stabilize the intrinsic (Cu vacancy) doping of chalcocite. TiO_2 was identified as a particularly

promising interfacial layer, especially when grown subsequent to at least one ALD cycle of Al_2O_3. Under these conditions, a carrier concentration on the order of 10^{17} was stabilized for at least 2 weeks under ambient conditions without further encapsulation. XPS analysis reveals no evidence for Cu at the exposed surface of TiO_2 under these optimal processing conditions. In situ thin-film growth and conductivity measurements suggest that the role of the TMA/H_2O treatment is not as a barrier but rather to reduce the Cu_2S carrier concentration and improve the nucleation of subsequent TiO_2 growth. Room-temperature steady-state PL studies reveal band edge emission characteristic of stoichiometric Cu_2S that is most intense when the absorber layer is sandwiched between ZrO_2 under- and overlayers. When TiO_2 and/or NiO interfaces are introduced, the PL intensity is significantly reduced, behavior consistent with charge-transfer quenching. Together, these studies demonstrate the potential for utilizing related Cu_2S nanolaminate stacks in stable photovoltaics.

■ ASSOCIATED CONTENT

Ⓢ Supporting Information

Additional XPS, QCM, and PL data. This material is available free of charge via the Internet at http://pubs.acs.org.

■ AUTHOR INFORMATION

Corresponding Author

*E-mail: martinson@anl.gov.

Present Addresses

[§]High Energy Physics, Argonne National Laboratory, 9700 South Cass Avenue, Argonne, Illinois 60439, United States.
[∥]Euclid Techlabs, LLC, 5900 Harper Road, Solon, Ohio 44139, United States.
[⊥]Department of Chemical Engineering and Materials Science, University of Minnesota, 421 Washington Avenue South East, Minneapolis, Minnesota 55455, United States.
[#]Department of Mechanical Engineering, University of Minnesota, 111 Church Street South East, Minneapolis, Minnesota 55455, United States.

Notes

The authors declare no competing financial interest.

■ ACKNOWLEDGMENTS

S.C.R. was supported in part by the Department of Energy (DOE) Office of Energy Efficiency and Renewable Energy (EERE) Postdoctoral Research Awards under the EERE Solar Program administered by the Oak Ridge Institute for Science and Education (ORISE) for the DOE. ORISE is managed by Oak Ridge Associated Universities (ORAU) under DOE contract no. DE-AC05-06OR23100. The research was performed at Argonne National Laboratory, a U.S. Department of Energy Office of Science Laboratory operated under contract no. DE-AC02-06CH11357 by UChicago Argonne, LLC. Use of the Center for Nanoscale Materials was supported by the U.S. Department of Energy, Office of Science, Office of Basic Energy Sciences, under contract no. DE-AC02-06CH11357. The authors thank Richard D. Schaller (NST, Argonne National Laboratory) for his assistance with the PL measurements.

■ ABBREVIATIONS USED

ALD, atomic-layer deposition
TMA, trimethylaluminum
TTIP, titanium tetraisopropoxide
TiTDMA, tetrakis(dimethylamido)titanium(IV)
CuAMD, bis(*N*,*N*′-disec-butylacetamidinato)dicopper(I)
NiAMD, nickel amidinate
PL, photoluminescence
XPS, X-ray photoelectronspectroscopy
QCM, quartz crystal microbalance
I−*V*, current−voltage

■ REFERENCES

(1) Boer, K. W. *J. Cryst. Growth* **1982**, *59*, 111−120.
(2) Böer, K. W. *Phys. Status Solidi A* **1977**, *40*, 355−384.
(3) Böer, K. W. *Phys. Status Solidi A* **1981**, *66*, 11−43.
(4) Henry, C. H. *J. Appl. Phys.* **1980**, *51*, 4494−4500.
(5) Lukashev, P.; Lambrecht, W.; Kotani, T.; van Schilfgaarde, M. *Phys. Rev. B* **2007**, *76*, 195202-1−195202-14.
(6) Shockley, W.; Queisser, H. J. *J. Appl. Phys.* **1961**, *32*, 510−519.
(7) Bragagnolo, J. A.; Barnett, A. M.; Phillips, J. E.; Hall, R. B.; Rothwarf, A.; Meakin, J. D. *IEEE Trans. Electron Devices* **1980**, *27*, 645−651.
(8) Hall, R. B. *Appl. Phys. Lett.* **1981**, *38*, 925−926.
(9) Matsumoto, H.; Nakayama, N.; Yamaguchi, K.; Ikegami, S. *Jpn. J. Appl. Phys.* **1976**, *15*, 1849−1850.
(10) Matsumoto, H.; Nakayama, N.; Yamaguchi, K.; Ikegami, S. *Jpn. J. Appl. Phys.* **1977**, *16*, 1283−1284.
(11) Rastogi, A. C.; Salkalachen, S. *Sol. Cells* **1983**, *9*, 185−202.
(12) Al-Dhafiri, A. M.; Russell, G. J.; Woods, J. *Semicond. Sci. Technol.* **1992**, *7*, 1052−1057.
(13) Potter, R. W. *Econ. Geol.* **1977**, *72*, 1524−1542.
(14) Sands, T. D.; Washburn, J.; Gronsky, R. *Phys. Status Solidi A* **1982**, *72*, 551−559.
(15) Okamoto, K.; Kawai, S. *Jpn. J. Appl. Phys.* **1973**, *12*, 1130−1138.
(16) Martinson, A. B. F.; Riha, S. C.; Thimsen, E.; Elam, J. W.; Pellin, M. J. *Energy Environ. Sci.* **2013**, *6*, 1868−1878.
(17) Adams, D.; Alford, T. L.; Rafalski, S. A.; Rack, M. J.; Russell, S. W.; Kim, M. J.; Mayer, J. W. *Mater. Chem. Phys.* **1996**, *43*, 145−152.
(18) Liu, C. J.; Jeng, J. S.; Chen, J. S.; Lin, Y. K. *J. Vac. Sci. Technol., B* **2002**, *20*, 2361−2366.
(19) Riha, S. C.; Johnson, D. C.; Prieto, A. L. *J. Am. Chem. Soc.* **2011**, *133*, 1383−1390.
(20) Lotfipour, M.; Machani, T.; Rossi, D. P.; Plass, K. E. *Chem. Mater.* **2011**, *23*, 3032−3038.
(21) Machani, T.; Rossi, D. P.; Golden, B. J.; Jones, E. C.; Lotfipour, M.; Plass, K. E. *Chem. Mater.* **2011**, *23*, 5491−5495.
(22) McBrayer, J. D. *J. Electrochem. Soc.* **1986**, *133*, 1242−1246.
(23) Lee, W.; Cho, H.; Cho, B.; Kim, J.; Kim, Y.-S.; Jung, W.-G.; Kwon, H.; Lee, J.; Reucroft, P. J.; Lee, C.; Lee, J. *J. Electrochem. Soc.* **2000**, *147*, 3066−3069.
(24) Li, X. N.; Liu, L. J.; Zhang, X. Y.; Chu, J. P.; Wang, Q.; Dong, C. *J. Electron. Mater.* **2012**, *41*, 3447−3452.
(25) Liu, C. J.; Chen, J. S.; Lin, Y. K. *J. Electrochem. Soc.* **2004**, *151*, G18−G23.
(26) Liu, G.; Schulmeyer, T.; Thissen, A.; Klein, A.; Jaegermann, W. *Appl. Phys. Lett.* **2003**, *82*, 2269−2271.
(27) Tai, Y.-H.; Chiu, H.-L.; Chou, L.-S. *J. Electrochem. Soc.* **2012**, *159*, J200−J203.
(28) Thimsen, E.; Baryshev, S. V.; Martinson, A. B. F.; Elam, J. W.; Veryovkin, I. V.; Pellin, M. J. *Chem. Mater.* **2013**, *25*, 313−319.
(29) Liu, Y.; Gibbs, M.; Perkins, C. L.; Tolentino, J.; Zarghami, M. H.; Bustamante, J.; Law, M. *Nano Lett.* **2011**, *11*, 5349−5355.
(30) ten Cate, S.; Liu, Y.; Suchand Sandeep, C. S.; Kinge, S.; Houtepen, A. J.; Savenije, T. J.; Schins, J. M.; Law, M.; Siebbeles, L. D. A. *J. Phys. Chem. Lett.* **2013**, *4*, 1766−1770.
(31) Liu, Y.; Tolentino, J.; Gibbs, M.; Ihly, R.; Perkins, C. L.; Liu, Y.; Crawford, N.; Hemminger, J. C.; Law, M. *Nano Lett.* **2013**, *13*, 1578−1587.
(32) Martinson, A. B. F.; Elam, J. W.; Pellin, M. J. *Appl. Phys. Lett.* **2009**, *94*, 123107-1−123107-3.
(33) George, S. M. *Chem. Rev.* **2010**, *110*, 111−131.

(34) Goodman, C. H. L.; Pessa, M. V. *J. Appl. Phys.* **1986**, *60*, R65−R81.
(35) Puurunen, R. L. *J. Appl. Phys.* **2005**, *97*, 121301-1−121301-52.
(36) Leskelä, M.; Ritala, M. *Angew. Chem., Int. Ed.* **2003**, *42*, 5548−5554.
(37) Dasgupta, N. P.; Mack, J. F.; Langston, M. C.; Bousetta, A.; Prinz, F. B. *Rev. Sci. Instrum.* **2010**, *81*, 044102-1−044102-6.
(38) Thimsen, E.; Martinson, A. B. F.; Elam, J. W.; Pellin, M. J. *J. Phys. Chem. C* **2012**, *116*, 16830−16840.
(39) Riha, S. C.; Libera, J. A.; Elam, J. W.; Martinson, A. B. F. *Rev. Sci. Instrum.* **2012**, *83*, 094101-1−094101-8.
(40) Zinovev, A. V.; Moore, J. F.; Hryn, J.; Pellin, M. J. *Surf. Sci.* **2006**, *600*, 2242−2251.
(41) Liu, C. J.; Chen, J. S. *J. Vac. Sci. Technol., B* **2005**, *23*, 90−95.
(42) Barnett, A. M.; Devaney, W. E.; Storti, G. M.; Meakin, J. D. *IEEE Trans. Electron Devices* **1978**, *25*, 377−379.
(43) Fahrenbruch, A. L.; Bube, R. H. *J. Appl. Phys.* **1974**, *45*, 1264−1275.
(44) Gill, W. D. *J. Appl. Phys.* **1970**, *41*, 3731−3738.
(45) Bagge-Hansen, M.; Outlaw, R. A.; Seo, K.; Reece, C. E.; Spradlin, J.; Manos, D. M. *J. Vac. Sci. Technol., A* **2011**, *29*, 053001-1−053001-3.
(46) Goswami, A.; Trehan, Y. N. *Proc. Phys. Soc., Sect. B* **1957**, *70*, 1005−1008.
(47) Brelle, M. C.; Torres-Matinez, C. L.; McNulty, J. C.; Mehra, R. K.; Zhang, J. Z. *Pure Appl. Chem.* **2000**, *72*, 101−118.
(48) Kriegel, I.; Jiang, C.; Rodríguez-Fernández, J.; Schaller, R. D.; Talapin, D. V.; da Como, E.; Feldmann, J. *J. Am. Chem. Soc.* **2012**, *134*, 1583−1590.
(49) Luther, J. M.; Jain, P. K.; Ewers, T.; Alivisatos, A. P. *Nat. Mater.* **2011**, *10*, 361−366.
(50) Zhao, Y.; Burda, C. *Energy Environ. Sci.* **2012**, *5*, 5564−5576.
(51) Zhao, Y.; Pan, H.; Lou, Y.; Qiu, X.; Zhu, J.; Burda, C. *J. Am. Chem. Soc.* **2009**, *131*, 4253−4261.
(52) Mulder, B. J. *Phys. Status Solidi A* **1972**, *13*, 79−88.
(53) Xu, Q.; Huang, B.; Zhao, Y.; Yan, Y.; Noufi, R.; Wei, S.-H. *Appl. Phys. Lett.* **2012**, *100*, 061906-1−061906-4.
(54) Elam, J. W.; Martinson, A. B. F.; Pellin, M. J.; Hupp, J. T. *Chem. Mater.* **2006**, *18*, 3571−3578.
(55) Elam, J. W.; Baker, D. A.; Hryn, A. J.; Martinson, A. B. F.; Pellin, M. J.; Hupp, J. T. *J. Vac. Sci. Technol., A* **2008**, *26*, 244−252.
(56) Liu, Y.; Shen, S.; Brillson, L. J.; Gordon, R. G. *Appl. Phys. Lett.* **2011**, *98*, 122907-1−122907-3.
(57) Abdulagatov, A. I.; Yan, Y.; Cooper, J. R.; Zhang, Y.; Gibbs, Z. M.; Cavanagh, A. S.; Yang, R. G.; Lee, Y. C.; George, S. M. *ACS Appl. Mater. Interfaces* **2011**, *3*, 4593−4601.
(58) Pawlowski, M.; Zabierowski, P.; Bacewicz, R.; Marko, H.; Barreau, N. *Thin Solid Films* **2011**, *519*, 7328−7331.
(59) Trupke, T.; Nyhus, J.; Haunschild, J. *Phys. Status Solidi RRL* **2011**, *5*, 131−137.
(60) Pankove, J. I. *Sol. Cells* **1980**, *2*, 443−449.
(61) Li, L. Q.; Liu, Z. F.; Li, M.; Hong, L.; Shen, H.; Liang, C. L.; Huang, H.; Jiang, D.; Ren, S. *J. Phys. Chem. C* **2013**, *117*, 4253−4259.
(62) Bhide, V. G.; Salkalachen, S.; Rastog, A. C.; Rao, C. N. R.; Hegde, M. S. *J. Phys. D: Appl. Phys.* **1981**, *14*, 1647−1656.